Gravity and anisotropy effects in the volume determination of Si spheres for the kilogram realisation

Gravity and anisotropy effects in the volume determination of Si spheres for the kilogram realisation

D Mari[1], A Nicolaus[2], E Kuhn[2], N Kuramoto[3], G Mana[1] and E Massa[1]

[1]INRIM – Istituto Nazionale di Ricerca Metrologica, Strada delle Cacce 91, 10135 Torino, Italy
[2]PTB Physikalisch-Technische Bundesanstalt, Bundesallee 100, 38116 Braunschweig, Germany
[3]NMIJ – National Metrology Institute of Japan, National Institute of Advanced Industrial Science and Technology, 1-1-1 Umezono, Tsukuba, Ibaraki 305-8563, Japan

Email: d.mari@inrim.it

Abstract: Counting ^{28}Si atoms plays a fundamental role in the realisation of the unit of mass in terms of stipulated values of fundamental physical constants. In this realisation, the measurement of the volume of ^{28}Si sphere is a fundamental step. This paper reports about a finite element analysis of the self-weight effect on the volume determination, taking the crystal anisotropy into account. The sphere volume might be overestimated from 0.3×10^{-9} to 5.1×10^{-9} (relative terms), depending on the crystal orientation and measurement procedure.

Keywords: kilogram realisation, self-weight, finite element analysis, anisotropy.

1. Introduction

The 26th General Conference on Weights and Measures (16th November 2018) adopted a revision of the International System of Units (SI). It is effective since May 2019 [1] and is based on stipulated values of several fundamental physical constants. From now on, the mass unit, the kilogram, is realised – with fractional uncertainties of few parts in 10^8 – by two methods [2]: the so-called Kibble balance [3] and X-Ray-Crystal-Density (XRCD) [4]. The XRCD experiment relies on counting the atoms in a perfect-crystal ^{28}Si sphere having known volume, lattice parameter, surface properties, isotopic composition, and chemical purity [5-7]. A significant contribution to the counting uncertainty is the volume measurement [8-10].

The sphere diameter is about 93.7 mm, corresponding to a mass close to 1 kg. Since the form error is less than 100 nm, the volume is determined as $\pi D^3/6$, where D is the mean diameter. In previous work, we reported about a finite element analysis [11, 12] of the self-weight effect on the volume determination at the National Metrology Institute of Japan (NMIJ), where an isotropic model was used. In this paper, we build on this analysis, take the silicon anisotropy into account and extend the study to the measurement set-up of the Physikalisch Technische Bundesanstalt (PTB).

2. Volume determination

The interferometric measurement of the sphere volume requires two steps. The first is the measurement of the distance, l, between the end surfaces of a stable optical etalon. The second is the measurement of the gaps, l_1 and l_2, between the sphere and the etalon end-surfaces [5]. The diameter, $D = l - (l_1 + l_2)$, is obtained by difference and averaged over many measurement directions.

As shown in Fig. 1, the NMIJ uses a fused-quartz Fabry–Perot etalon enclosed in a vacuum chamber equipped with active temperature control. The three aluminium pins (4 mm diameter, 2 mm tip radius, and PEEK-coated) support the sphere. They are placed at 120° azimuthal distances and 128.8° polar angle (38.8° latitude south). The interferometer senses the sphere diameter in the horizontal (equatorial) plane. As described in [12], the azimuth difference between the beam axes and the nearest pins is set to 30° to minimise the deformation of the measured diameter. A two-axis rotation mechanism repositions the sphere to measure the diameters in directions distributed as uniformly as possible: more than 10^3 diameter values are collected and averaged, with the same angle between each measured diameter and the supports. The uncertainty of the mean diameter (not corrected for the phase shift due to the surface oxide layer) is 0.62 nm, to which a fractional uncertainty of 6.6 nm/m will correspond [6].

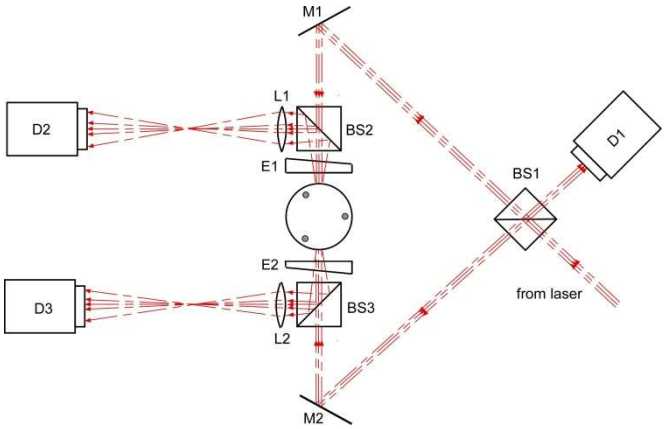

Figure 1. Schematic of NMIJ set-up; BS: beam splitter, D1, D2, and D3: CCD detectors, M: mirror, E1 and E2: etalon flats. The sphere rests on three supporting pins (grey dots).

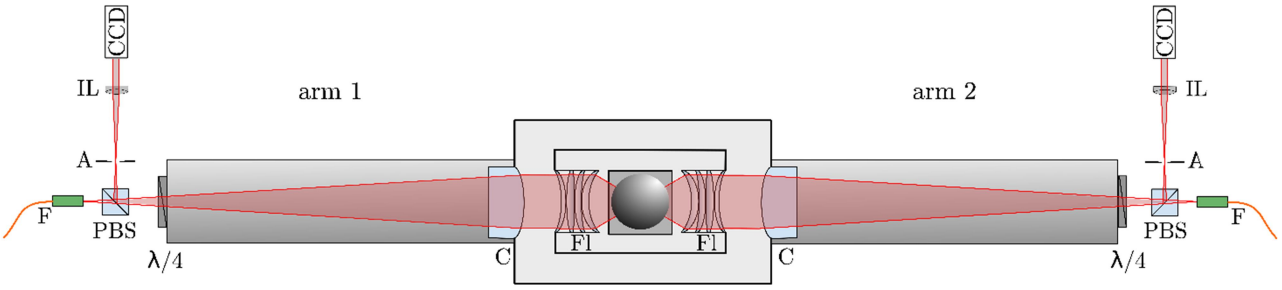

Figure 2. Schematic of PTB set-up; F: fibre, PBS: polarising beam splitter, A: aperture, CCD: camera (512 × 512 pixels), IL: imaging lens, C: Collimator, FL: Fizeau lens.

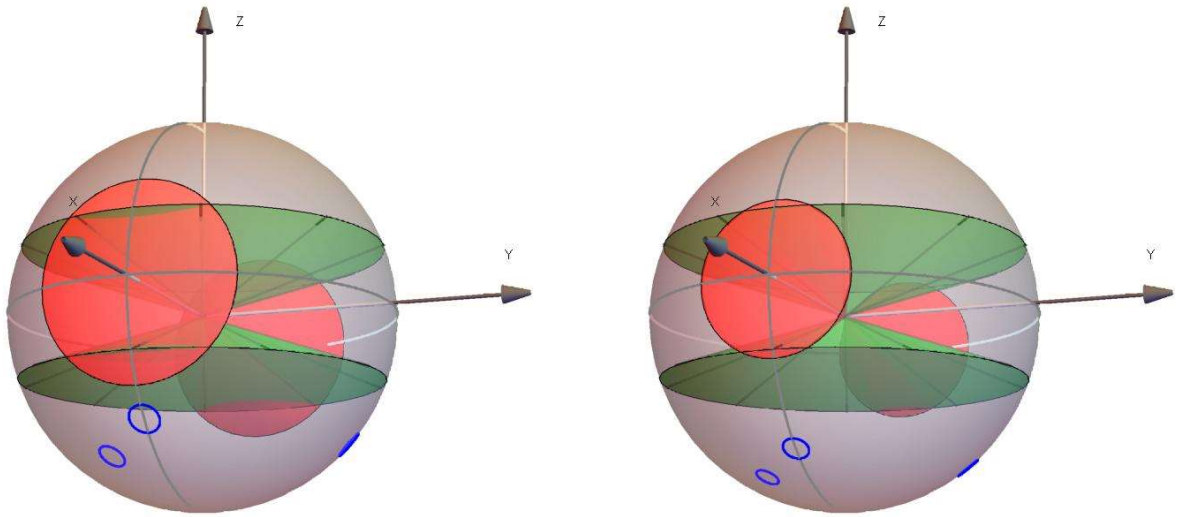

Figure 3. Measurement geometries of the PTB's interferometers 1 (left) and 2 (right). The supporting pins (blue circles) are at 40° (left) and 50° south (right) latitude and spaced by 120° azimuth. The zero meridian (grey) goes through the first pin and beam axis. The azimuths are positive in the counterclockwise direction. The measured diameters are inside the red cones having 60° (left) or 45° (right) apertures. The green cones collect the diameters at 20° north latitude (see also Fig. 6 left, violet line).

As shown in Fig. 2, the PTB uses spherical interferometers [9]: the etalon end-surfaces form a spherical cavity surrounding the sphere. The etalon is placed in a vacuum chamber equipped with active temperature control. The sphere is supported by three PEEK flats placed at 120° azimuthal distance and 130° (interferometer 1) or 140° (interferometer 2) polar angle (40° or 50° latitude south). Lenses expand and match the incoming beams to the cavity and sphere, focusing them to the cavity centre. Therefore, the relationship $D = l - (l_1 + l_2)$ holds over the full 60° (interferometer 1) or 45° (interferometer 2) field of view. The beam axes are in the horizontal (equatorial) plane, have the same azimuth of one of the supports and bisect the opposite two. Figure 3 shows the geometries of the PTB's measurements.

An orientation device rotates the sphere about two axes; the surface is thus covered with about 30 patches. For each orientation, the gaps l_1 and l_2 are simultaneously measured in about 10^4 (interferometer 1) or 10^6 (interferometer 2) directions. The equal thickness interference patterns (deviations are less than $\lambda/10$ within the full field of view) allow high-resolution measurements of small differences of l, l_1, and l_2 from their nominal values. This iterated process enables a high-resolution topography of the whole sphere. The fractional uncertainty of the mean diameter (not corrected for the phase shift due to the surface oxide layer) is 0.2 nm, to which a fractional uncertainty of 2.3 nm/m will correspond.

3. Finite element analysis

3.1 Finite element model

Since silicon is anisotropic, the values of Young modulus, E_i (the stress to strain ratio in the same crystallographic direction i), and the Poisson ratio, ν_{ij} (the negative ratio between the strains in the direction j and that in an orthogonal direction i of uniform stress), depend on the sphere orientation, see Figs. 4 and 5. The Poisson ratio is a function of three angular coordinates: two identify the stress direction, the last the (orthogonal) direction of the transverse strain. Since, the ν_{ij} domain is a 3-sphere (the boundary of a ball in four dimensions), in each point of the 2-spheres in Fig. 5 there is a circle (Hopf fibration, not shown) associated with the missing last coordinate.

The silicon density was set to 2329 kg m^{-3}, the gravity acceleration to 9.807 m s^{-2}, and the sphere diameter to 0.093720266 m. About 5×10^5 tetrahedral elements formed the mesh. Since fixed translational and rotational degrees of freedom (Dirichlet boundary conditions on the surface elements) result in non-physical effects, we merged the sphere into the supports by generating a composite object (formed by connected domains of different materials (silicon and PEEK and sharing the boundaries between the neighbours) and prescribed Dirichlet conditions on the backside support-elements. The total contact area on the three supports, 0.076 mm^2 (NMIJ interferometer), 0.65 mm^2 (PTB interferometer 1), and 0.73 mm^2 (PTB interferometer 2), were estimated through the Hertz theory of spherical indentation [13]. Namely, the depth of the indentation and radius of each single contact area are $h = a^2/(2R)$ and $a = \sqrt[3]{3FR/(4E^*)}$, where $1/E^* = (1-\nu_1^2)/E_1 + (1-\nu_2^2)/E_2$, R is the sphere radius, F is the load component orthogonal to the support, and E_1, E_2 and ν_1, ν_2 are the Young moduli and Poisson ratios of (isotropic) silicon (160 GPa and 0.23) and PEEK (3.6 GPa and 0.38).

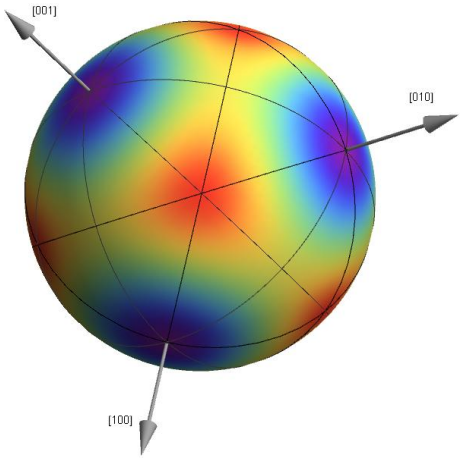

Figure 4. Map of the Young modulus, the ratio between uniform stress in different crystallographic directions and the strain in the same direction. The arrows are ⟨100⟩ directions. The colour scale is from 1.3 GPa (violet, ⟨100⟩ directions) to 1.9 GPa (red, ⟨111⟩ directions). The (spherical) triangle tiling highlights the underlying octahedral symmetry.

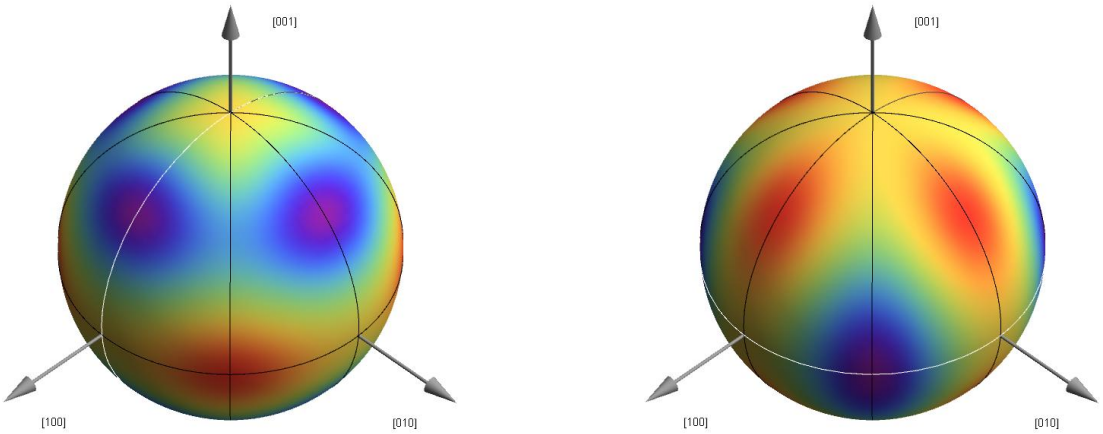

Figure 5. Maps of the Poisson ratio vs the stress direction, where the transverse-strain directions are on the same meridians (left) and the equator (right). The colour scale is from 0.06 (violet, the stress and strain are both in ⟨110⟩ orthogonal directions) to 0.36 (red, the stress is in a ⟨110⟩ direction, the strain is in a ⟨001⟩ one). The arrows are ⟨100⟩ directions. The Poisson ratio is shown as a scalar field over the Hopf fibration of a 3-sphere, where great circles on the 3-sphere (the loci of the transverse-strain directions) map into the points of the imaged 2-sphere (the loci of the stress directions).

3.2 Isotropic model

A previous study of the NMIJ set-up [12], simplified the analysis of the self-weight deformation by assuming isotropy. Since $-\varepsilon_j = \nu_{ij}\varepsilon_i \propto \nu_{ij}/E_i$, where ε_j and ε_i are strains in the direction j and in an orthogonal direction i of uniform stress, the ν/E isotropic ratio was set to the ν_{ij}/E_i average over all the crystallographic directions, 1.42×10^{-3} GPa^{-1}, with E = 160 GPa and ν = 0.228. In [12], we checked that, with the isotropy assumption and axially symmetric constraints, the self-weight deformation is axially symmetric as expected: the deviations from a constant of the diameters having the same polar angle are less than 1 pm.

Before facing the anisotropic problem, we applied the isotropic model also to the PTB interferometers. Figure 6 shows the results of the finite element analysis. The azimuths of the axes of the two beams are 0° and 180°. The three supports induce a three-fold rotational symmetry, which is more evident at higher elevation angles. Since the diameters are identified by their northern extreme (elevation angle), the indentations manifest themselves at the 60°, 180°, and 300° azimuths, where the south extreme of the diameter approaches the supports, see Fig. 3.

To investigate the numerical accuracy of the calculated strains (estimated to be 1%), we checked the 3-fold rotational symmetry of the sphere deformation. Figure 7 shows the sample standard-deviations of triples of diameters. The diameters of each triple have the same elevation and are spaced by 120°.

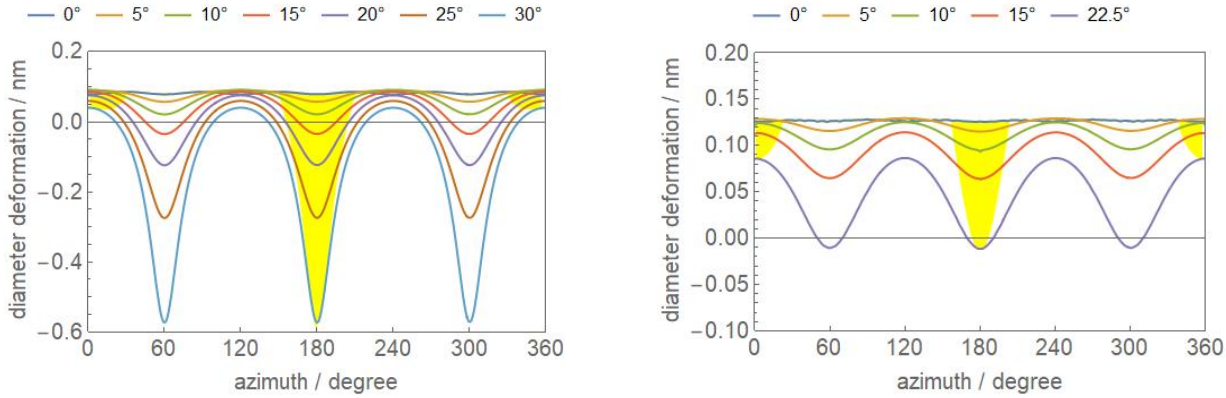

Figure 6. PTB interferometers, isotropic model. Deformation of the sphere diameter due to gravity, as a function of azimuth and at different elevation angles, for the interferometer 1 (left) and 2 (right). Positive deformations indicate larger diameters. The support azimuths are 0°, 120°, and 240°; the beam-axis azimuths are 0° and 180°. The elevation angles (top labels) refer to the latitude of the northern extreme of the diameters, see Fig. 3. Hence, the indentations manifest themselves at the 60°, 180°, and 300° azimuths, where the south extreme approaches the supports. The yellow regions indicate the diameters in the interferometer field-of-view.

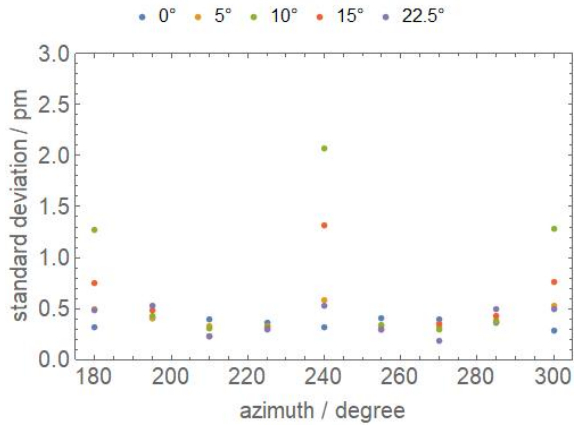

Figure 7. PTB interferometer 2, isotropic model. Sample standard-deviations of the triple of diameters. The diameters of each triple have the same elevation (from 0° to 22.5°, top labels) and are spaced by 120°. The support azimuths are 0°, 120°, and 240°. The elevation angles refer to the latitude of the northern extreme of the diameters, see the green cones in Fig. 3. Similar results hold for the interferometer 1.

3.3 Anisotropic model

We extended the analysis by taking the anisotropy into account for both the NMIJ and PTB set-ups and measurement procedures. The not-null elements of the stiffness matrix are given in table 1 for the [100], [010], [001] crystal orientation.

To identify the orientation of the sphere, we specify the crystallographic directions of the vertical (*z*-axis) and *x*-axis (the axis crossing the equatorial projection of the first pin). To make the analysis as simple as possible, we considered only four orientations; they are listed in table 2. The stiffness matrices relevant to each orientation were obtained by transforming Si(100) matrix into the new (rotated) coordinates. They were implemented into the finite element model according to [14, 15]. For example, to obtain the stiffness matrix for the Si(110) orientation, we rotated the Si(100) one – given in table 1 – by 45° about the [001] axis.

Figure 8 shows the radial deformation of the sphere for the PTB interferometers and Si(311) orientation of the sphere. The support indentations, which are made asymmetric by the anisotropy and amount to more than 1 nm, were excluded from the map. Equatorial ridges are visible midway the indentations. In the field of view, deformations range from –0.84 nm to 0.11 nm (interferometer 1) and from –1.01 nm to 0.14 nm (interferometer 2). Figure 9 shows the results for PTB interferometers. The sphere-diameter deformations for the NMIJ set-up are very similar to the ones of the PTB's interferometer 1. As expected, the Si(100) and Si(111) orientations are the most stretchy and stiffest ones.

Table 3 summarises the self-weight effects on the diameter and volume measurements. For the PTB measurements, we considered the mean elongation of the diameters in opposite spherical sectors having 60° (interferometer 1) and 45° (interferometer 2) apertures and axis lying in the equatorial plane with azimuths equal to 0° and 180° (see fig. 3). We also considered the mean elongation of the diameters in opposite sectors having 60° (interferometer 1) and 45° (interferometer 2) apertures and axis lying in the equatorial plane with azimuths equal to 30° and 210°. This last choice maximises the distance of the beam axes from the supports. For the NMIJ measurements, we considered a single equatorial diameter having 30° azimuth, which is the diameter measured in each of the NMIJ repositionings.

The fractional errors of the sphere volume range from 0.3×10^{-9} (PTB interferometer 1, orientation Si(111)) to 5.1×10^{-9} (PTB interferometer 2, orientation Si(100)). The mean fractional errors are 1.2×10^{-9} (interferometer 1) to 3.9×10^{-9} (interferometer 2). Nearly identical values are obtained for the azimuth of the laser beam equal to 30° and the isotropic case. In the NMIJ case, the mean fractional error is 2.6×10^{-9}, confirming the value obtained in the previous isotropic study [12].

Table 1. Not-null elements of the stiffness matrix for Si crystals [14]. The measurement unit is GPa.

c_{11}, c_{22}, c_{33}	c_{12}, c_{13}, c_{23}	c_{44}, c_{55}, c_{66}
165.7	63.9	79.6

Table 2. Crystal orientations.

orientation	*x*-axis (first pin axis)	*y*-axis	*z*-axis (vertical)
Si(100)	010	001	100
Si(110)	001	$1\bar{1}0$	110
Si(311)	$01\bar{1}$	$2\bar{3}\bar{3}$	311
Si(111)	$01\bar{1}$	$2\bar{1}\bar{1}$	111

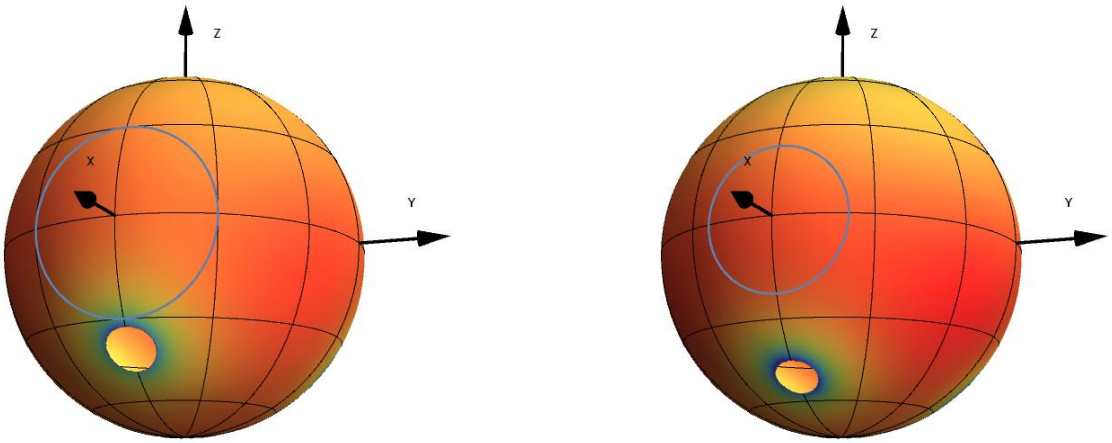

Figure 8. Maps of the radial deformation of the sphere. PTB interferometers 1 (left) and 2 (right), crystal orientation Si(311), see table 2. The colour scale is from –1.01 nm (violet) to 0.14 nm (red). Due to the large deformation, the contact areas are excluded from the map. The blue circle defines the measurement area, see Fig. 3.

Table 3. Summary of the finite element analysis

	PTB interferometer 1, contact area 0.65 mm^2		PTB interferometer 2, contact area 0.73 mm^2	
	laser beam azimuth 0°			
	$\Delta D_{60}/D$	$\Delta V_{60}/V$	$\Delta D_{45}/D$	$\Delta V_{45}/V$
Si(100)	6.9×10^{-10}	2.1×10^{-9}	1.7×10^{-9}	5.1×10^{-9}
Si(110)	4.2×10^{-10}	1.3×10^{-9}	1.3×10^{-9}	3.9×10^{-9}
Si(311)	3.8×10^{-10}	1.1×10^{-9}	1.3×10^{-9}	3.9×10^{-9}
Si(111)	1.1×10^{-10}	0.3×10^{-9}	0.8×10^{-9}	2.4×10^{-9}
mean	4.0×10^{-10}	1.2×10^{-9}	1.3×10^{-9}	3.9×10^{-9}
isotropic case	3.3×10^{-10}	1.0×10^{-9}	1.1×10^{-9}	3.3×10^{-9}
	laser beam azimuth 30°			
	$\Delta D_{60}/D$	$\Delta V_{60}/V$	$\Delta D_{45}/D$	$\Delta V_{45}/V$
Si(100)	7.1×10^{-10}	2.1×10^{-9}	1.4×10^{-9}	2.2×10^{-9}
Si(110)	5.1×10^{-10}	1.5×10^{-9}	1.3×10^{-9}	3.9×10^{-9}
Si(311)	4.2×10^{-10}	1.3×10^{-9}	1.2×10^{-9}	3.6×10^{-9}
Si(111)	2.2×10^{-10}	0.7×10^{-9}	0.8×10^{-9}	2.4×10^{-9}
mean	4.7×10^{-10}	1.4×10^{-9}	1.2×10^{-9}	3.6×10^{-9}
isotropic case	4.5×10^{-10}	1.4×10^{-9}	1.2×10^{-9}	3.6×10^{-9}

NMIJ interferometer, laser beam azimuth 30°, contact area 0.076 mm^2

	$\Delta D/D$	$\Delta V/V$
Si(100)	1.2×10^{-9}	3.6×10^{-9}
Si(110)	0.9×10^{-9}	2.7×10^{-9}
Si(311)	0.8×10^{-9}	2.4×10^{-9}
Si(111)	0.6×10^{-9}	1.8×10^{-9}
mean	0.9×10^{-9}	2.6×10^{-9}
isotropic case	0.9×10^{-9}	2.6×10^{-9}

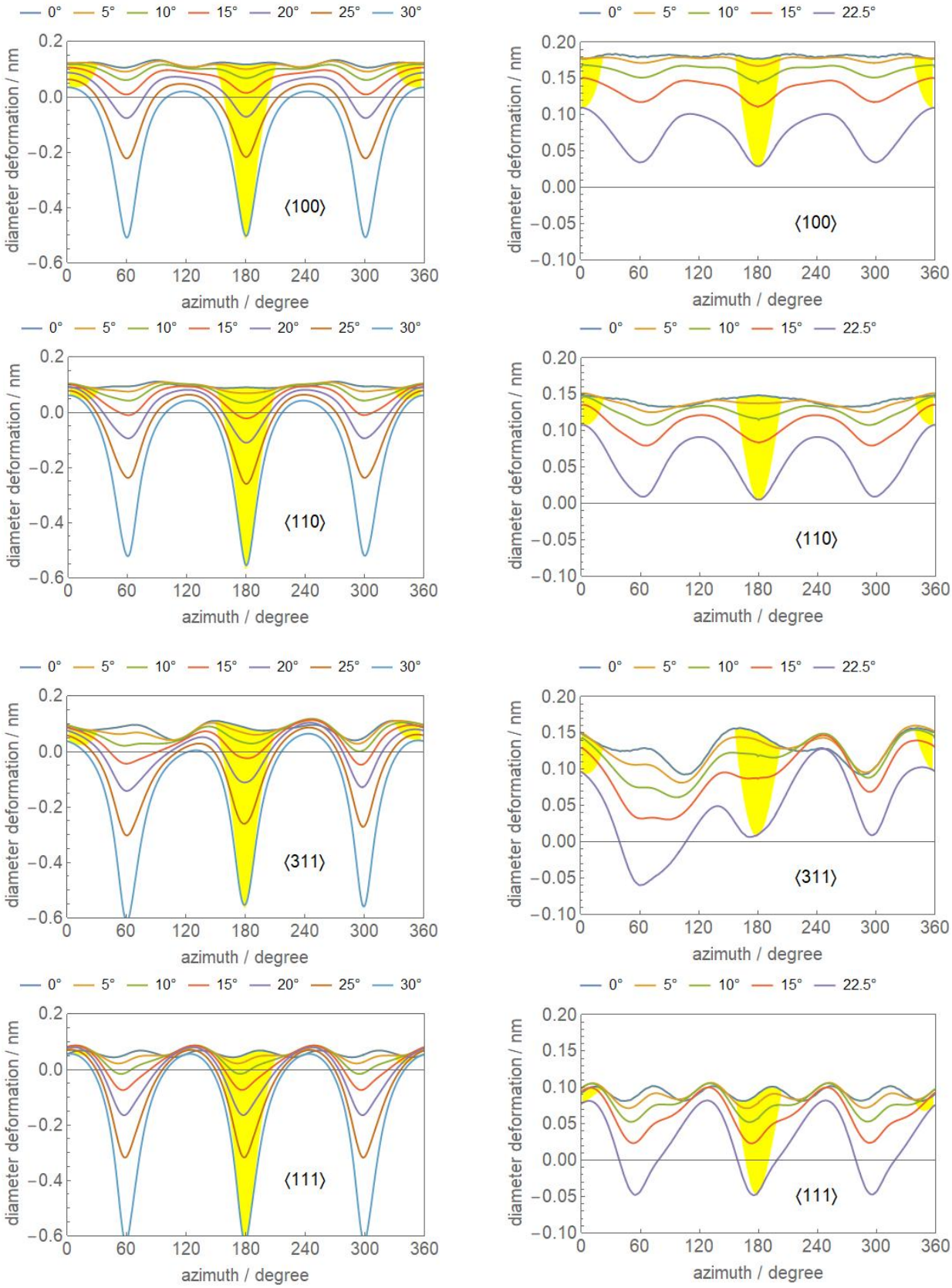

Figure 9. PTB interferometers, anisotropic model. Self-weight deformation of the sphere diameters, as a function of azimuth and at different elevation angles, for the PTB interferometers 1 (left) and 2 (right). The Miller indexes are the directions along the vertical; the crystal orientations in the horizontal plane are according to table 2. Positive deformations indicate larger diameters. The support azimuths are 0°, 120°, and 240°; the beam-axis azimuths are 0° and 180°. The elevation angles (top labels) refer to the latitude of the northern extreme of the diameters, see Fig. 3. Hence, the indentations manifest themselves at the 60°, 180°, and 300° azimuths, where the south extreme approaches the supports. The yellow regions indicate the diameters in the interferometer field-of-view.

To investigate the uncertainty on the volume determination originated by the stress concentration at the contact area between the Si sphere and supports, Fig. 10 shows the mean elongation of the diameters in the field of view of the PTB's interferometers as a function of the contact area and of the PEEK Young-modulus. As already observed in the NMIJ case [12], the equatorial diameters and the interferometer 2 measurement are not so much affected by the contact between the sphere and supports.

A fractional volume uncertainty of 4.5×10^{-9} seems possible [10]. Therefore, experimental verifications of the finite-element analysis are necessary. Figure 11 shows the maximum diameter difference predicted by our numerical analysis, when the measurement of the same diameter is repeated after rotating the sphere by 180° rotation about the axis of the laser beam. The maximum predicted difference occurs for the diameters having 30° north latitude and 0° and 180° azimuths, see Figs. 3, 6, and 8 (left). These differences range from 0.6 nm to 0.7 nm, depending on the assumed contact area, and might be experimentally detected in future experiments.

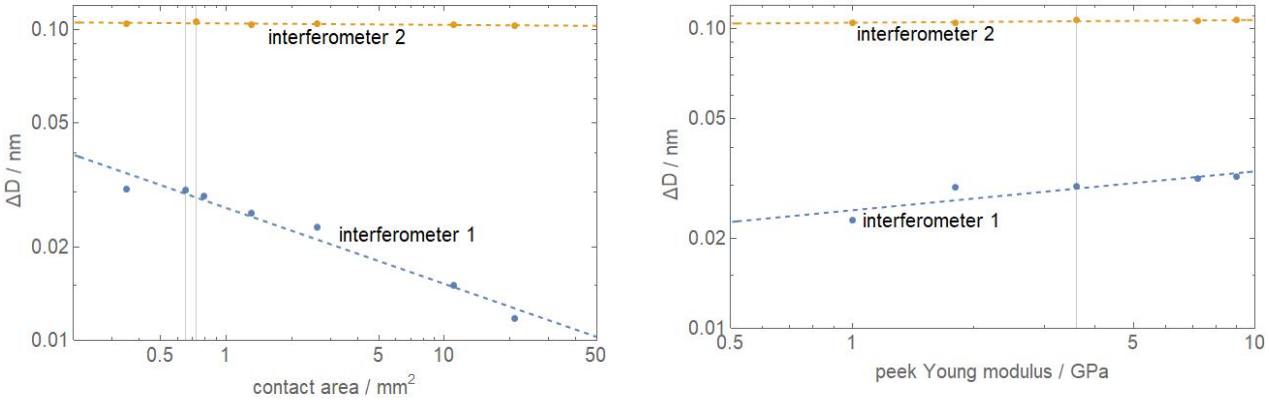

Figure 10. PTB interferometers, isotropic model. Log-log plot of the (predicted) mean elongation of the diameters in the interferometer field of view as a function of the contact area (left, the PEEK Young modulus is fixed to 3.6 GPa) and of the PEEK Young modulus (right, the Hertz theory determines the contact area). The vertical lines indicate the contact areas and Young modulus used in the analysis. Dashed lines are the best power-law fits to the data.

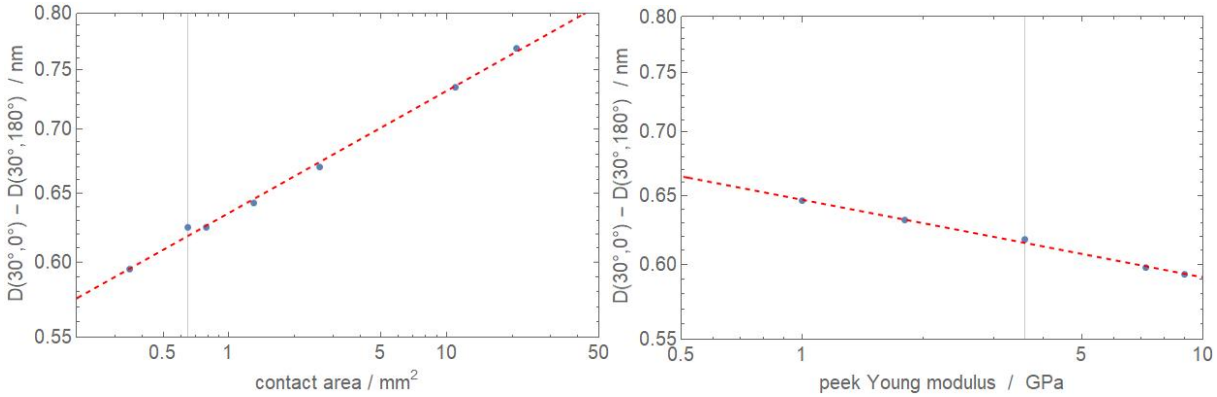

Figure 11. PTB interferometer 1, isotropic model. Log-log plot of the (predicted) maximum diameter difference when measurements are repeated with the upside-down sphere (180° rotation about the axis of the laser beam). Left: the PEEK Young modulus is fixed to 3.6 GPa. Right: the Hertz theory determines the contact area. The maximum difference occurs for the diameters having 30° north latitude and 0° and 180° azimuths, see Figs. 3, 6, and 8 (left). The vertical lines indicate the contact area and Young modulus used in the analysis. Dashed lines are the best power-law fits to the data.

4. Conclusions

We studied the effect of the self-weight and anisotropy on the volume determination of silicon spheres, which is an input datum for the kilogram and mole realisations by counting atoms.

The finite element model used took both the NMIJ and PTB set-ups and procedures into account. To reduce the computational load, we considered only four different crystal orientations. In the NMIJ case, we averaged four diameters: each in the equatorial plane and having 30° azimuth, but with a different crystal orientation [8]. In the PTB case, we averaged (after reorientation) all the diameters in opposite spherical sectors having 60° (interferometer 1) and 45° (interferometer 2) apertures [9].

Our results show fractional volume-overestimations equal to 2.6×10^{-9} (NMIJ interferometer), 1.2×10^{-9} (PTB interferometer 1), and 3.9×10^{-9} (PTB interferometer 2). These values are comparable with

those obtained using isotropic models. The greatest correction required by the PTB interferometer 2 is due to the high south latitude of the sphere supports and the reduced interferometer field of view. This measurement geometry moves the field of view away from the indentations, but the increased equatorial bulge due to the load on the lower support and the removal of the shrank diameters near the indentations bias the average diameter positively. By moving the support toward the equator, the equatorial deformation changes from bulging to shrinking. In the isotropic case, there exists an optimal support latitude, about at 29° south, where equatorial strain is null [12].

References

[1] Bureau International des Poids et Mesures The International System of Units (S) 9th edition 2019, available online at https://www.bipm.org/en/publications/si-brochure/
[2] Bettin H and Schlamminger S 2016 Realization, maintenance and dissemination of the kilogram in the revised SI *Metrologia* **53** A1-A5
[3] Robinson I A and Schlamminger S 2016 The watt or Kibble balance: a technique for implementing the new SI definition of the unit of mass *Metrologia* **53** A46-A74
[4] Fujii K *et al*., 2016 Realization of the kilogram by the XRCD method *Metrologia* **53** A19-A45
[5] Azuma Y *et al.* 2015 Improved measurement results for the Avogadro constant using a ^{28}Si-enriched crystal *Metrologia* **52** 360-375
[6] Kuramoto N *et al.* 2017 Determination of the Avogadro constant by the XRCD method using a ^{28}Si-enriched sphere *Metrologia* **54** 716-729
[7] Bartl G *et al.* 2017 A new ^{28}Si single crystal: counting the atoms for the new kilogram definition, *Metrologia* **54** 693-715.
[8] Kuramoto N et al. 2017 Volume measurements of ^{28}Si-enriched spheres using an improved optical interferometer for the determination of the Avogadro constant *Metrologia* **54** 193-203
[9] Nicolaus A, Bartl G, Peter A, Kuhn E and Mai T 2017 Volume determination of two spheres of the new ^{28}Si crystal of PTB *Metrologia* **54** 512-515
[10] Mai T and Nicolaus A 2017 Optical simulation of the new PTB sphere Interferometer *Metrologia* **54** 487-493
[11] COMSOL Multiphysics® 5.2a
[12] Mari D, Massa E, Kuramoto N and Mana 2018 G Self weight effect in the measurement of the volume of silicon spheres *Metrologia* **55** 294-301
[13] Johnson K L 1987 *Contact Mechanics* Cambridge University Press
[14] Lin Zhang, Raymond Barrett, Peter Cloetens, Carsten Detlefs and Manuel Sanchez del Rio 2014 Anisotropic elasticity of silicon and its application to the modelling of X-ray optics *Journal of Synchrotron Radiation* **21** 507-517
[15] COMSOL Multiphysics® 5.3a